IOPscience iopscience.iop.org

Home Search Collections Journals About Contact us My IOPscience

The calculation of some thermoelastic properties and pressure–temperature (*P*–*T*) diagrams of Rh and Sr using molecular dynamics simulation

This article has been downloaded from IOPscience. Please scroll down to see the full text article.

2007 J. Phys.: Condens. Matter 19 326204

(http://iopscience.iop.org/0953-8984/19/32/326204)

View the table of contents for this issue, or go to the journal homepage for more

Download details:
IP Address: 129.252.86.83
The article was downloaded on 28/05/2010 at 19:57

Please note that terms and conditions apply.

IOP PUBLISHING JOURNAL OF PHYSICS: CONDENSED MATTER

J. Phys.: Condens. Matter **19** (2007) 326204 (13pp) doi:10.1088/0953-8984/19/32/326204

The calculation of some thermoelastic properties and pressure–temperature (P–T) diagrams of Rh and Sr using molecular dynamics simulation

Y O Ciftci[1,3], K Colakoglu[1], S Ozgen[2] and S Kazanc[2]

[1] Department of Physics, Faculty of Arts and Sciences, Gazi University, 06500 Ankara, Turkey
[2] Department of Physics, Faculty of Arts and Sciences, Firat University, 23119 Elazig, Turkey

E-mail: yasemin@gazi.edu.tr

Received 6 April 2007, in final form 15 June 2007
Published 13 July 2007
Online at stacks.iop.org/JPhysCM/19/326204

Abstract

In this study, molecular dynamics simulations are carried out using a modified many-body Morse potential function in the framework of the embedded-atom method (EAM). Pressure–temperature (P–T) diagrams are determined for Rh and Sr. For the metals the bulk moduli are calculated from the pressure versus volume curves, and specific heats are calculated from the enthalpy versus temperature curves. The temperature and pressure dependence of the elastic constants and bulk moduli are also calculated for Rh and Sr. The obtained results are in good agreement with the available experimental data.

1. Introduction

Computer simulations on various metallic systems usually use simple pairwise potentials. However, the interactions in real metallic materials cannot be represented only by simple pairwise interactions. A pure pairwise potential model gives the Cauchy relation, $C_{12} = C_{44}$, between the elastic constants, which is not the case in real metals. Therefore, many-body interactions should be taken into account in any studies of metals and metal alloys.

It is very important to calculate the phase diagrams of metallic systems and their alloys in order to achieve technological improvements. The phase diagrams are still obtained by using experimental techniques because there are no available methods for entirely theoretical predictions of all of the phase diagrams of any pure metal. Therefore, in the calculations of the phase diagrams some expressions have been formed by using theoretical or semi-empirical approach, and their validity has been investigated in a selected portion of the phase diagrams. The expressions suggested in semi-empirical approaches generally contain some factors depending on temperature and pressure. Therefore, the calculated phase region is restricted by experimental limits. Nowadays, however, free-energy concepts, such as Gibbs and Helmholtz, have been widely used to calculate the macroscopic phase diagrams [1, 2] in

[3] Author to whom any correspondence should be addressed.

which thermodynamic parameters are dominant. In the microscopic scale, their calculations require some vibrational properties which can be derived from elastic constants of the material. So, the correct calculations of the elastic constants are important as well as the calculations of phase diagrams.

Molecular dynamics (MD) simulations can be utilized to compute the thermodynamic parameters and the results of the external effects, such as temperature and pressure or stress acting on a physical system [3, 4]. In the MD simulations, the interatomic interactions are modelled with a suitable mathematical function, and its gradient gives the forces between atoms. Hence, Newton's equations of motion of the system are solved numerically and the system is forced to be in a state of minimum energy, an equilibrium point of its phase space. Although many properties of the system, such as enthalpy, cohesive energy and internal pressure, have been directly calculated in MD simulations, the entropy which is required for the free-energy calculations has not been directly obtained, but it is possible to obtain it by some approaches involving harmonic or anharmonic assumptions. There are some investigations related to these approaches: the calculation of the free energy between face-centred cubic (FCC) and hexagonal close-packed (HCP) structures [5, 6], the investigation of the first-order phase transition [7], the dependence of the phase diagram on the range of attractive intermolecular forces [8], the investigation of harmonic lattice dynamics and entropy calculations in metals and alloys [9], the calculation of the P–T diagram of hafnium [10], etc. Recently, the P–T diagrams for Ni and Al have been calculated by Gurler and Ozgen [11] by using MD simulations based on the Sutton–Chen version of the EAM [12].

The reliability of the results obtained from MD simulations depends on the suitable modelling of the interatomic interactions. Interatomic interactions are usually results of fits to various experimental data at 0 K or room temperature. However, it is not clear whether simulations performed at other temperatures still reproduce the experimental data accurately. Comparing theoretical and experimental elastic constants and other properties at various temperatures can serve as a measure of reliability and usefulness of potential models [13, 14]. In fact, there are several potential energy functions that can be used for metallic systems. However, the EAM, originally developed by Daw and Baskes [15, 16] to model the interatomic interactions of FCC metals, has been successfully used to compute the properties of metallic systems such as bulk, surface and interface problems. The reliability of the EAM in the bulk and its simple form for use in computer simulations make it attractive.

In this study, in order to model Rh and Sr metallic systems we have used the EAM functions modified by two of us (Ciftci and Colakoglu [17]), developed first by Cai [18]. In this work, we have carried out MD simulations to obtain the P–V diagrams at 300 K and the P–T diagrams of the systems for an ideal FCC lattice with 1372 atoms, by using an anisotropic MD scheme. In addition, the bulk modulus and specific heat of the system in the solid phase are determined, and result-driven simulations are interpreted by comparing with the values in the literature. We have also calculated the temperature dependences of the elastic constants and bulk moduli for Rh and Sr. The results obtained are compared with the values in the literature.

2. Potential energy function

According to the embedded-atom method, the cohesive energy of an assembly of N atoms is given by [15, 16]

$$E_{\text{tot}} = \sum_i F_i(\rho_i) + \sum_{i>j} \phi(r_{ij}) \tag{1}$$

$$\rho_i = \sum_{j(\neq i)} f(r_{ij}), \tag{2}$$

Table 1. The experimental properties and potential parameters of Rh and Sr. The experimental properties: lattice parameters (a_0) at room temperature is from [20], bulk modulus (B_m) and elastic constants (C_{ij}) given at zero temperature are from [21], the vacancy formation energy (E_v^f) is from [22], the melting temperature (T_m) is from [23], and the specific heat C_p is from [24]. The arbitrary constants (m and n), α, β, D_1 and D_2 are the calculated potential parameters.

	a_0 (Å)	r_0 (Å)	E_c (eV)	E_v^f (eV)	B_m (GPa)	C_{11} (GPa)	C_{12} (GPa)	C_{44} (GPa)	T_m (K)	C_p (J mol^{-1} K^{-1})
Rh	3.8044	2.6901	5.75	1.90	268.63	422.0	192.0	194.0	2237.0	25.0
Sr	6.0849	4.3027	1.72	0.66	11.6	15.3	10.3	9.9	1042.0	26.0

	m	n	α (Å^{-1})	β	D_1 (eV)	D_2 (eV)
Rh	5.0	0.2	1.5374	4.1584	0.4931	3.6119
Sr	3.0	0.5	1.2737	4.8076	0.1039	1.6142

where E_{tot} is the total cohesive energy, ρ_i is the host electron density at the location of atom i due to all other atoms, $f(r_{ij})$ is the electronic density function of an atom, r_{ij} is the distance between atoms i and j, $F_i(\rho_i)$ is the embedding energy to embed atom i in an electron density ρ_i, and $\phi(r_{ij})$ is the pairwise potential energy function between atoms i and j.

In this work, we used a modified pairwise potential function in the framework of the Cai version [18] of the EAM. The present form of the potential makes it more flexible owing to the constants, m and n, in the multiplier forms. Such a factor included in the classical Morse function is treated by Verma and Rathore [19] to compute the phonon frequencies of Th, based on the central pair potential model. The modified parts of the potential and the other terms are as follows:

$$f(r) = f_e e^{-\alpha(r-r_e)}, \tag{3}$$

$$F(\rho) = -F_0\left[1 - \ln\left(\frac{\rho}{\rho_e}\right)^n\right]\left(\frac{\rho}{\rho_e}\right)^n + D_2\left(\frac{\rho}{\rho_e}\right), \tag{4}$$

$$\phi(r) = \frac{D_1}{(m-1)}\left[\frac{e^{-m\beta(\frac{r}{r_e}-1)}}{(\beta\frac{r}{r_e})^n} - \left(\beta\frac{r}{r_e}\right)^n e^{-\beta(\frac{r}{r_e}-1)}\right], \tag{5}$$

where α, β, D_1 and D_2 are fitting parameters that are determined by the lattice parameter a_0, the cohesive energy E_c, the vacancy formation energy E_v^f, and the elastic constants C_{ij}. Here ρ_e is the host electron density at the equilibrium state, r_e is the nearest-neighbour equilibrium distance, and $F_0 = E_c - E_v^f$. In this potential model, there are four parameters: β and D_1 are from the two-body term, and m and n are adjustable selected constants. The fitting parameters are determined by minimizing the value of $W = \sum[(X^{cal} - X^{exp})/X^{exp}]^2$. Here X represents the calculated and experimental values of the quantities taken into account in the fitting process. Hence, the potential functions can be fitted very well to the experimental properties of the matter, such as the vacancy formation energy, cohesive energy, elastic constants, and lattice constant (a_0) in an equilibrium state. In the fitting process here, the cutoff distance is taken to be $r_{cut} = 1.65a_0$. In equation (3), the f_e parameter is selected as unity for monatomic systems because it is used for alloy modelling as an adjustable parameter to constitute suitable electron density. For the selected values of the constants m and n, the computed potential parameters and experimental input data for Rh and Sr are given in table 1.

The cohesive energy changes with the variation of lattice constants of Rh and Sr calculated from equation (1) and from the general expression of the cohesive energy of metals proposed

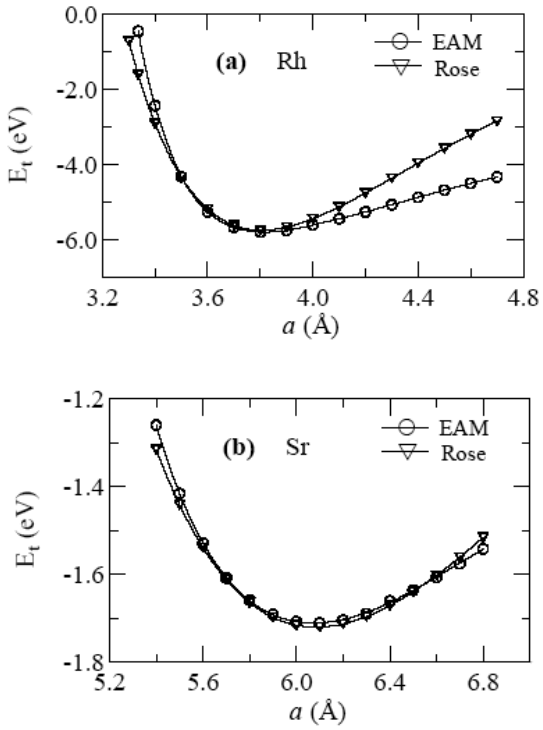

Figure 1. Rose and EAM energies versus lattice constant for (a) Rh and (b) Sr.

by Rose *et al* [25] are compared in figure 1. The Rose energy is also called the generalized equation of state of metals and is written as

$$E_{\mathrm{R}}(a^*) = -E_0(1 + a^*)\mathrm{e}^{-a^*} \tag{6}$$

$$a^* = \left(\frac{a}{a_0} - 1\right) \Big/ \left(\frac{E_{\mathrm{C}}}{9B_{\mathrm{m}}\Omega}\right)^{1/2}, \tag{7}$$

where E_0 is a constant to be taken as an equilibrium cohesive energy of solid, B_{m} is the bulk modulus, and Ω is the atomic volume in equilibrium. It has been determined that the cohesive energies calculated from equation (1) with the parameter given in table 1 for Rh and Sr are in good agreement with Rose energies in equilibrium.

3. Molecular dynamics simulation

The Lagrange function for an anisotropic box containing N particles, i.e. an MD cell, given by Parrinello and Rahman, is [26, 27]

$$L_{\mathrm{PR}} = \tfrac{1}{2}\sum_{i=1}^{N} m_i(\dot{\mathbf{s}}_i^{\mathrm{t}}\mathbf{G}\dot{\mathbf{s}}_i) - E_{\mathrm{tot}} + \tfrac{1}{2}M\ \mathrm{Tr}(\dot{\mathbf{h}}^{\mathrm{t}}\dot{\mathbf{h}}) - P_{\mathrm{ext}}V, \tag{8}$$

where m_i is the mass of particle i, $\mathbf{s}_i$ is the scaled coordinate of atom i and is represented by a column vector whose elements are between zero and unity, $\mathbf{h} = (\mathbf{a}, \mathbf{b}, \mathbf{c})$; $\mathbf{a}$, $\mathbf{b}$ and $\mathbf{c}$ vectors are MD cell axes, the metric tensor $\mathbf{G}$ is given by matrix product $\mathbf{h}^t\mathbf{h}$, M is an arbitrary constant which represents the mass of the computational box, P_{ext} is the external pressure applied on

the cell, and V is the volume of the MD cell and is obtained from det(**h**). Thus, the square of the distance between particles i and j is described by $r_{ij}^2 = \mathbf{s}_{ij}^{\mathrm{t}}\mathbf{G}\mathbf{s}_{ij}$. The classical equations of motion of the system obtained from equation (1) become

$$\ddot{\mathbf{s}}_i = -\frac{1}{m_i}\mathbf{F}_i - \mathbf{G}^{-1}\dot{\mathbf{G}}\dot{\mathbf{s}}_i \tag{9}$$

$$\ddot{\mathbf{h}} = M^{-1}(\mathbf{\Pi} - \mathbf{I}P_{\mathrm{ext}})\boldsymbol{\sigma}, \tag{10}$$

where $\boldsymbol{\sigma} = (\mathbf{b}\times\mathbf{c}, \mathbf{c}\times\mathbf{a}, \mathbf{a}\times\mathbf{b}) = V(\mathbf{h}^{\mathrm{t}})^{-1}$ and the microscopic stress tensor, $\mathbf{\Pi}$, is a dyadic given as follows:

$$\mathbf{\Pi} = V^{-1}\left[\sum_{i=1}^{N} m_i\mathbf{v}_i\mathbf{v}_i - \sum_{i=1}^{N}\sum_{j>i}^{N}\frac{F_{ij}}{r_{ij}}\mathbf{r}_i\mathbf{r}_i\right]. \tag{11}$$

Also, the force on an atom i in the system is calculated from the following equation:

$$\mathbf{F}_i = -\nabla_s E_i = -\sum_{\substack{j=1\\ j\neq i}}^{N}\left[F_i'\rho_j' + F_j'\rho_i' + \phi_{ij}'\right]\frac{\hat{\mathbf{s}}_{ij}}{r_{ij}}, \tag{12}$$

where the primes denote the first derivatives of the functions with respect to their arguments.

In all of the simulation studies, the equations of motion given in equations (9) and (10) were numerically solved by using the velocity version of the Verlet algorithm [28]. The size of the integration step was chosen to be 1.97×10^{-15} s for Rh and 6.35×10^{-15} s for Sr. Initial structures of the systems were constructed on a lattice with 1372 atoms and an FCC unit cell. It has been observed that, with these initial conditions, the systems were equilibrated in 5000 integration steps. Time averages of the thermodynamic properties of the system in each simulation run were determined by using 30 000 integration steps following the equilibration of the system. The structures of the system in the solid phase were examined by using the radial distribution function, $g(r)$. Melting temperatures were determined from the plots of the cohesive energy versus temperature. It is possible to classify our simulation runs in two groups as thermal and pressure applications. In the thermal applications, the temperature of the system under zero pressure is raised from 100 to 4600 K for Rh (and 100 to 2900 K for Sr) with an increment of 100 K in each run of 35 000 integration step; but near the melting temperatures, the increment is reduced to 20 K. The pressure applications are also implemented by repeating the thermal applications under pressure values of 0.5, 1.0, 1.5, 2.5, 5.0, 7.5, 10.0, 15.0 and 20.0 GPa. In each run, the simulation was restarted with different pressure to avoid algorithmic errors.

The temperature dependence of the elastic constants and the bulk moduli are calculated by following the procedure given by Karimi *et al* [13]. The fluctuation formula for the calculation of the elastic constants in the *EhN* (E is the total energy, h is a matrix representing the volume and shape of the computational cell and N is total number of particles) ensemble was derived in [29] as follows:

$$C_{ijkm} = -\frac{V_0}{k_{\mathrm{B}}T}(\langle P_{ij}P_{km}\rangle - \langle P_{ij}\rangle\langle P_{km}\rangle) + \frac{2Nk_{\mathrm{B}}T}{V_0}(\delta_{ik}\delta_{jm} + \delta_{im}\delta_{jk}) + \langle B1_{ijkm}\rangle + \langle B2_{ijkm}\rangle + \langle B3_{ijkm}\rangle. \tag{13}$$

Here, P_{ij} is the microscopic stress tensor for the EAM functions which can be determined from the virial theorem (see [13]). The first term on the right-hand side in equation (13) is called the fluctuation term, the second the temperature correction and the last three are called the Born terms. Pair terms in the EAM function are included in $B1$ and $B2$ while many-body contributions are in $B3$. The details of the formulations for the fluctuation terms and Born terms

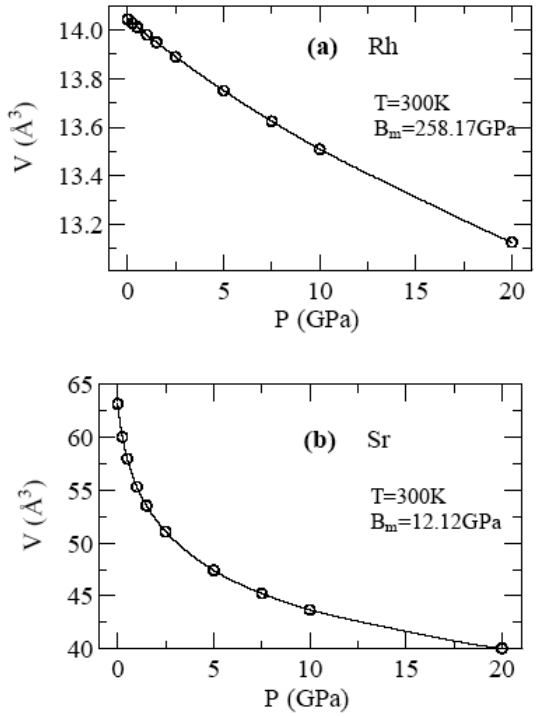

Figure 2. P–V diagrams for (a) Rh and (b) Sr.

used in the calculations are given in [13, 29]. We have used 30 000 integration steps (time after equilibration) to calculate the elastic constants and bulk moduli in the 0–1000 K temperature range, under zero pressure.

4. Results and discussion

We will classify our results into eight different categories:

(i) the P–V diagram has been analysed to determine the bulk modulus under zero pressure,
(ii) the changes of the lattice constant with temperature have been investigated to determine the coefficient of linear thermal expansion,
(iii) the specific heat has been determined by using the changes of the enthalpy with temperature,
(iv) the radial distribution function has been obtained in solid and liquid phases for the estimation of structural properties,
(v) the P–T graph, which is plotted by using the variation in melting temperatures with increasing pressure acted on the system, has been examined,
(vi) the variation of the elastic constants and bulk moduli with temperature are, also, determined,
(vii) the pressure dependence of V/V_0 has been obtained, and finally
(viii) the pressure dependence of the elastic constants has been investigated.

The change of the atomic volume with the gradually increasing pressure, which acts on the system at 300 K, is given in figures 2(a) and (b) for Rh and Sr. The bulk moduli calculated from

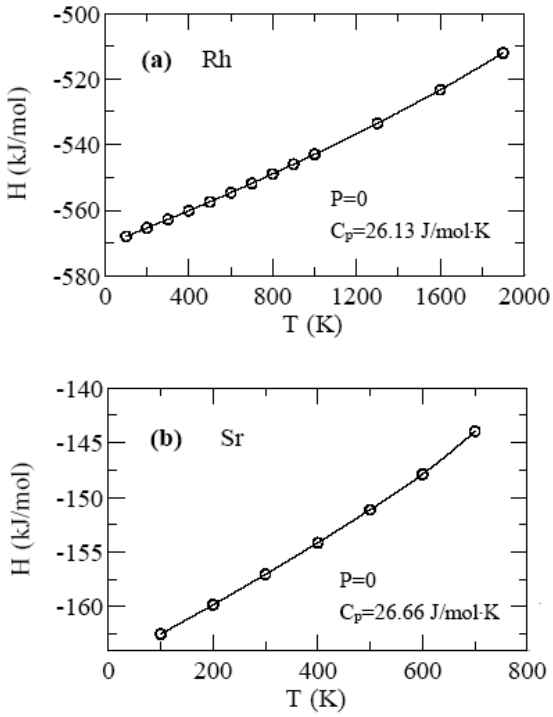

Figure 3. Variation of the enthalpy with temperature for (a) Rh and (b) Sr.

the P–V diagram shown in figure 2 are obtained as $B_{m\mathrm{Rh}} = 258.16$ and $B_{m\mathrm{Sr}} = 12.11$ GPa for Rh and Sr, respectively. The calculated bulk moduli are in good agreement with their experimental values (see table 1) within an error of ∼4.05% for Rh and ∼3.78% for Sr. The bulk modulus is a parameter which is used directly for determining the parameters of the potential energy functions. Therefore, it is an expected result that the values of the calculated bulk modulus have a minor error less then 4%. The errors on the values of the calculated bulk modulus are also maximum with respect to those of the others, apart from the calculated melting temperature, which is not included in the fitting process of the parameters of the potential energy functions.

The variations of enthalpy with temperature under zero pressure for solid Rh and Sr are given in figures 3(a) and (b), respectively, and these graphs are used to compute specific heats under the constant pressure. The calculated values of specific heats over 0–300 K are found to be $C_{p\mathrm{Rh}} = 26.13$ and $C_{p\mathrm{Sr}} = 26.66$ J mol^{-1} K^{-1} for Rh and Sr, respectively. Considering the experimental data in table 1, it can be seen that the specific heats are calculated with an error of 4.3%, and 2.5% for Rh and Sr, respectively. Specific heats are not directly used experimental parameters in the fitting process of the parameters of the potential energy functions. They have also not been calculated directly during the simulations, using some technique including a thermal fluctuation formula, but calculated from thermodynamic considerations with the ratio $\Delta H/\Delta T$. Therefore, the fact that the specific heats are calculated with an error less that 4.5% is an important finding, which shows the validity of our potential function and its parameters.

There are several methods for determining the melting temperature of a crystal. In one of these methods, as done here, MD simulations are performed on the system at various

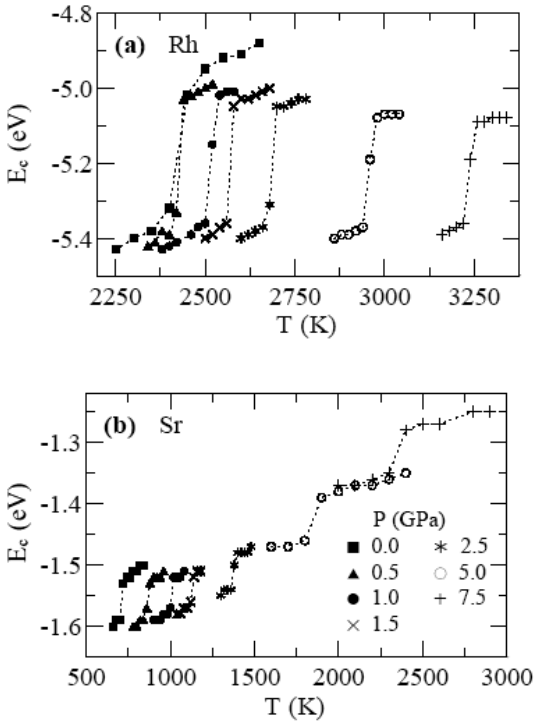

Figure 4. Changes of the cohesive energy as a function of temperature at different pressure for (a) Rh and (b) Sr. The symbols, ♦, ▲, ●, ×, ∗, ○, + represent the pressure values of 0.0, 0.5, 1.0, 1.5, 2.5, 5.0, 7.5 GPa, respectively.

temperatures, and the cohesive energy is plotted as a function of temperature. At the melting point, a discontinuity occurs in the cohesive energy. The other way of determining the melting temperature is to plot a caloric curve, which is the change of the total energy of crystal versus kinetic energy [30]. Indeed, the melting temperature of a metal is obtained as the temperature at which the Gibbs free energy of the solid and liquid phases becomes equal. The entropy is required to compute the free energy, but it cannot be directly calculated from MD simulations. For this reason, some other approaches are required [3]. Another way of determining the melting temperature is to simulate the solid–liquid interface [13]. In this way, the temperature for which the interface velocity goes to zero is determined as the melting temperature and it is reproduced more correctly than by way of the caloric curve. Karimi *et al* [13] estimated the melting temperature for Ni as 1630 ± 50 K within an error of −5.6%, using the solid–liquid interface technique.

In the present work, the variations of cohesive energy with temperature for different pressures acting on the system are given in figures 4(a) and (b) for Rh and Sr. We have computed the melting temperatures under zero pressure as 2380 ± 20 and 700 ± 20 K for Rh and Sr, respectively. When these values are compared with the experimental ones of 2237 and 1042 K given in table 1, the error for Rh becomes 6.39% and the error for Sr becomes −32.82%. From figure 1(a), it can be seen that the calculated cohesive energy values from our model are lower than the values of the Rose energy. According to the assumption that the Rose energies are correct, our model for Rh produces a deeper potential well for atoms. So, it can be interpreted that the error in the melting temperature for Rh results from the deepness of

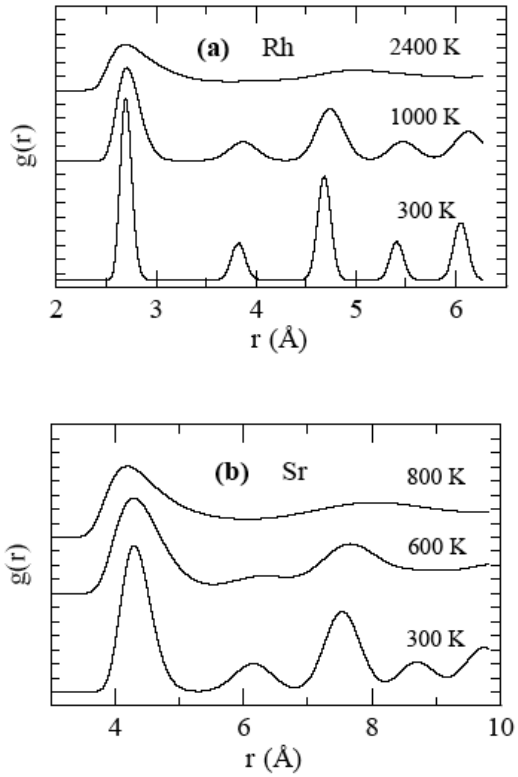

Figure 5. The radial distribution curves in solid and liquid phases for (a) Rh and (b) Sr.

the potential well, which depends mainly on the energy parameters D_1 and D_2 of the potential functions. However, as seen from figure 1(b) for Sr, our EAM version produces a shallow well for atoms. In this way, the calculated melting temperature of Sr is lower than the experimental one.

The radial distribution function is used to investigate the structural properties of the solid and liquid phases. The plot of radial distribution functions acquired in solid and liquid phases for Rh and Sr are given in figure 5. The first peak location of the radial distribution curves represents the distance of the nearest-neighbour atoms, r_0. The second peak location denotes the distances of next-nearest neighbours, a_0. These distances are found to be 2.699 and 3.816 Å, respectively for Rh. By comparing with experimental data given in table 1, the calculated errors in a_0 and r_0 are 0.3% for Rh. These distances are 4.297 and 6.164 Å, respectively, for Sr. By comparing with experimental data given in table 1, the present error in r_0 is 0.1% and it is 1.3% in a_0. So, the present errors can be omitted since the parameters of the potential energy function were fitted to the crystal properties in the static case. Since the peak locations shown in figures 5(a) and (b) satisfy certain peak locations at $\sqrt{2}$, $\sqrt{3}$, $\sqrt{4}$, $\sqrt{5}$, etc times r_0 in an ideal FCC unit cell, the metals have an FCC unit cell under zero pressure.

The P–T diagrams plotted by using the melting temperatures under different pressures are given in figures 6(a) and (b) for Rh and Sr, respectively. The binding energies of the metals can be reduced by increasing temperature. At high temperatures near the melting point, it is generally expected that the Gibbs free energy is lowered by a phase transition such as the martensitic type from one structure to another one which has lower energy at higher

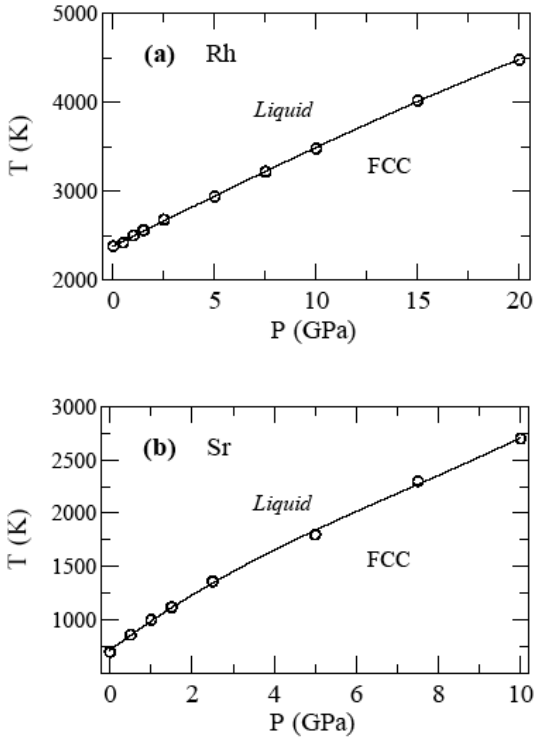

Figure 6. P–T diagrams for (a) Rh and (b) Sr.

Table 2. Elastic constants and bulk modulus of Rh calculated at 0, 300, 500, 700 and 1000 K as obtained from *NPT* MD simulation after 30 000 steps. For each temperature, the first number in the first row gives our MD result and the first number in the second row has been taken from [31]; for 0 K the second number (in parentheses) in the first row is the experimental value and the second number (in parentheses) in the second row is our static calculation result.

T (K)	C_{11} (GPa)	C_{12} (GPa)	C_{44} (GPa)	B (GPa)
0	343.94 (422.10)	192.17 (192.0)	187.81 (194.00)	242.76 (268.63)
	322.30 (363.75)	232.02 (202.31)	131.95 (197.96)	
300	314.48	175.95	169.53	232.58
	322.30 ± 0.66	223.02 ± 0.90	131.95 ± 0.69	256.11 ± 0.85
500	293.15	163.76	158.53	225.58
	312.03 ± 0.69	216.89 ± 0.44	124.72 ± 0.15	248.60 ± 0.52
700	269.92	150.25	148.51	218.28
	298.92 ± 0.77	210.23 ± 0.78	117.44 ± 0.14	239.79 ± 0.78
1000	237.63	133.51	130.92	206.83
	279.36 ± 1.12	199.07 ± 0.71	108.16 ± 1.07	225.83 ± 0.84

temperatures, like a body-centred cubic (BCC) lattice. However, we have not observed this type of phase transition for either Rh or Sr.

We calculated the temperature dependence of the elastic constants and bulk moduli of Rh and Sr by using MD simulations with 30 000 steps for each temperature considered in the range 0–1000 K. The results are summarized in tables 2 and 3 for Rh and Sr, respectively. For Rh the MD simulation results for the lattice parameter and cohesive energy at 0 K are 3.811 Å and

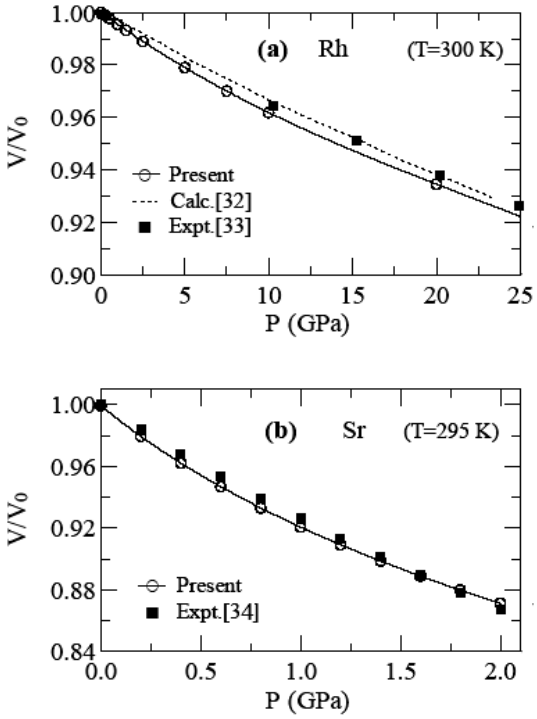

Figure 7. Variation of V/V_0 as a function of pressure for (a) Rh and (b) Sr.

Table 3. Elastic constants and bulk modulus of Sr calculated at 0, 300, 500, 700 and 1000 K as obtained from *NPT* MD simulation after 30 000 steps. For 0 K, the first number in the first row shows our MD results, and the second number (in parentheses) in the first row is the experimental values, while the numbers in the second row are the static calculation results.

T (K)	C_{11} (GPa)	C_{12} (GPa)	C_{44} (GPa)	B (GPa)
0	15.88 (15.30)	10.82 (10.36)	8.04 (9.90)	12.509 (11.6)
	15.58	10.66	7.89	
300	12.48	8.88	6.13	11.29
500	9.85	7.42	4.65	10.41
700	6.42	5.33	3.13	9.34
1000	3.62	3.61	0.35	7.02

5.790 eV, respectively. Simulation results show approximately 0.18% and 0.69% deviation from the experimental values of lattice parameter and cohesive energy, respectively. For Sr the same MD simulation results at 0 K are 6.078 Å and 1.711 eV, respectively. Simulation results for Sr show approximately 0.1% and 0.5% deviation from the experimental values of lattice parameter and cohesive energy, respectively. In these calculations the lattice parameters at 300 K are used as a reference. The errors in the cohesive energies and the lattice parameters have been found to be within the expected limits because their experimental values were utilized in the fitting process of the potential energy functions. Nonetheless, it is considered that the accuracy of these results necessitates not only having confidence in the potential energy functions and its parameters but also in the MD calculations.

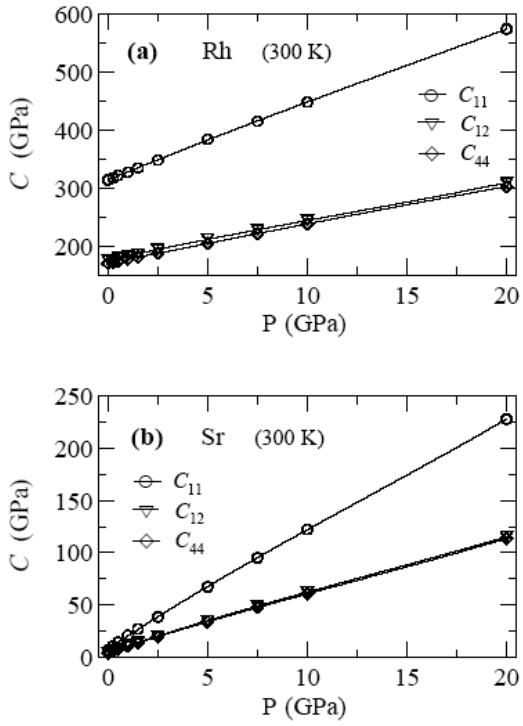

Figure 8. Variations of elastic constants with pressure for (a) Rh and (b) Sr.

The elastic constant values in tables 2 and 3 are closer to the experimental values, especially at 0 K, than those of [31].

We also calculated V/V_0 as a function of pressure (0–25 GPa) at 300 K for Rh and of pressure (0–2 GPa) at 295 K for Sr and added experimental points for comparing with MD results. The plots of V/V_0 versus pressure for the metals are given in figures 7(a) and (b). Here V_0 is the volume under the zero pressure. The MD results are in very good agreement with the experimental data and the curve calculated by Baria and Jani using pseudopotential theory [32].

Finally the variation of elastic constants with pressure for Rh and Sr is given in figure 8. Our calculated elastic constants are everywhere positive and smoothly increasing functions of pressure. This implies that Sr and Rh are mechanically stable crystals over the entire pressure range examined.

5. Conclusion

It has been found that the present version of the EAM with a recently developed potential function, which makes it more flexible owing to the parameter n, represents quite well the interactions between the atoms to simulate the studied monatomic systems. Since the parameterization technique of our potential is based on the bulk properties of metals at 0 K, it can in particular describe the temperature-dependent behaviours of our crystals qualitatively.

As a whole, the present model well describes the many physical properties, and our results are in reasonable agreement with the corresponding experimental findings, and provide another measure of the quantitative limitations of the EAM for bulk metals.

References

[1] Haasen P 1992 *Physical Metallurgy* 2nd edn (Cambridge: Cambridge University Press)
[2] Porter D A and Easterling K E 1992 *Phase Transformation in Metals and Alloys* 2nd edn (London: Chapman and Hall)
[3] Haile J M 1992 *Molecular Dynamics Simulation, Elementary Methods* (Canada: Wiley)
[4] Catlow C R A 1990 *Computer Modelling of Fluids, Polymers and Solids* ed C R A Catlow *et al* (Dordrecht: Kluwer) pp 1–28
[5] Moody M C and Ray J R 1986 *J. Chem. Phys.* **84** 1795
[6] Ihm J 1988 *Rep. Prog. Phys.* **51** 105
[7] Kerr W C, Hawthorne A M, Gooding R J, Bishop A R and Krumhansl J A 1992 *Phys. Rev.* B **45** 7036
[8] Hasegawa M and Ohno K 1997 *J. Phys.: Condens. Matter* **9** 3361
[9] Barrera G D and Tendler R H 1997 *Comput. Phys. Commun.* **105** 159
[10] Ostanin S A and Trubitsin V Y 2000 *Comput. Mater. Sci.* **17** 174
[11] Gurler Y and Ozgen S 2003 *Mater. Lett.* **57** 4336
[12] Finnis M W and Sinclair J E 1984 *Phil. Mag.* A **50** 45
[13] Karimi M, Stapay G, Kaplan T and Mostoller M 1997 *Modelling Simul. Mater. Sci. Eng.* **5** 337
[14] Erkoc S 1997 *Phys. Rep.* **278** 79
[15] Daw M S and Baskes M I 1983 *Phys. Rev. Lett.* **50** 1285
[16] Daw M S and Baskes M I 1984 *Phys. Rev.* B **29** 6443
[17] Ciftci Y O and Colakoglu K 2001 *Acta Phys. Pol.* A **100** 539
[18] Cai J and Ye Y Y 1996 *Phys. Rev.* B **54** 8398
[19] Verma M L and Rathore R P S 1994 *Phys. Status Solidi* b **185** 93
[20] Pearson W B 1967 *Handbook of Lattice Spacing and Structure of Metals and Alloys* (Oxford: Pergamon)
[21] Simmons R O and Wang H 1991 *Single Crystal Elastic Constants and Calculated Aggregate Properties, A Handbook* (Cambridge: MIT Press)
[22] *Londolt–Bornstein New Series* 1991 vols III-11 and III-18 (Berlin: Springer)
[23] Kittel C 1986 *Introduction to Solid State Physics* (New York: Wiley)
[24] Touloukian Y S and Buyco E H 1970 *Specific Heat: Metallic Elements and Alloys* (New York: IFI/Plenum)
[25] Rose J H, Smith J R, Guinea F and Ferrante J 1984 *Phys. Rev.* B **29** 2963
[26] Parrinello M and Rahman A 1980 *Phys. Rev. Lett.* **45** 1196
[27] Parrinello M and Rahman A 1981 *J. Appl. Phys.* 52 7182
[28] Verlet L 1967 *Phys. Rev.* **159** 98
[29] Wolf R J, Mansour K A, Lee M W and Ray J R 1992 *Phys. Rev.* B **46** 8027
[30] Nayak S K, Khanna S N, Rao B K and Jena P 1998 *J. Phys.: Condens. Matter* **10** 10853
[31] Cagin T, Dereli G, Uludogan M and Tomak M 1999 *Phys. Rev.* B **59** 3468
[32] Baria J K and Jani A R 2003 *Physica* B **328** 317
[33] Rice M H, McQueen R G and Walsh J H 1958 *Solid State Phys.* **6** 1 (from [31])
[34] Anderson M S, Swenson C A and Peterson D T 1990 *Phys. Rev.* B **41** 3329